

Two-Phase Flow Distribution in with Down-Scaling

Uttupulusu Surendra

NSRIT, Sontyam,
Andhra Pradesh 531173, India.

P.V.S. Murali Krishna

NSRIT, Sontyam,
Andhra Pradesh 531173, India.

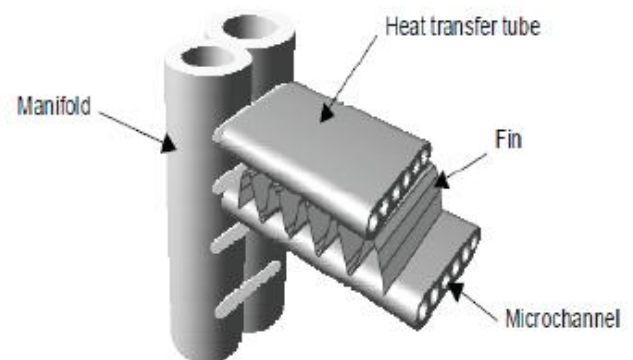
Introduction

The use of compact heat exchangers has increased over the last years due to the need for higher efficiency equipment in smaller package volumes. Lower operating costs because of rising energy prices has justified the larger initial cost of such heat exchangers. Making heat exchangers more compact involves reduction of channel hydraulic diameters and length of the flow channels.

Heat exchangers with MPE-tubes are now utilized in a growing number of applications, e.g. mobile and residential air conditioning. The good air and refrigerant-side performance of such heat exchangers has been documented extensively in the literature (Jacobi, 2001). Another advantage of microchannel heat exchangers (MCHE) is the possible charge reduction, often important in systems with flammable or poisonous refrigerants.

Generally, an implication of down-scaling the tube diameter is an increase in the number of parallel flow channels through the heat exchanger to keep the pressure loss at acceptable levels. The heat exchanger pressure losses affects the COP (Coefficient Of Performance) of the system. Because of the increasing number of parallel flow channels, the issue of fluid distribution has received growing attention.

One of the common assumptions in basic heat exchanger design theory has been that the fluids are distributed uniformly. In practice, a flow maldistribution often occurs, which can significantly reduce the performance of heat exchangers with parallel flow circuits.



1.2.Objective

To avoid the problems arising from maldistribution of refrigerant flow in heat exchanger manifolds, the behaviour of the fluid distribution must be understood. Capabilities of computer models for two-phase flows have been steadily improved over the last decades. However, it is not possible to achieve the necessary understanding of the complex two-phase flow involved in the manifold distribution problem without an experimental foundation. As a basis for developing new manifold designs to improve the heat exchanger performance, a better understanding of the flow within the manifold is of great importance. It was the intention of the current study to contribute to the understanding of the fundamental aspects involved in two-phase flow distribution.

Specific objectives of the work were to:

- Measure two-phase flow distribution in compact heat exchanger manifolds, with focus on manifolds in MPE-tube heat exchangers, at a range of realistic operating conditions.

Cite this article as: Uttupulusu Surendra & P.V.S. Murali Krishna, "Two-Phase Flow Distribution in with Down-Scaling", International Journal & Magazine of Engineering, Technology, Management and Research, Volume 5, Issue 12, 2018, Page 21-25.

- Investigate the performance of several manifold geometries, to enhance the understanding of the connection between two-phase flow distribution and the manifold geometry.
- analyse results, observations and findings in relation to other published models for two-phase flow distribution.
- Develop a model for two-phase flow distribution, which could be used in heat exchanger simulation models taking into account the performance reduction of flow maldistribution.
- Develop and demonstrate a heat exchanger simulation model and verify the modelling results against the laboratory experiments.

1.3. Outline of the thesis

Chapter 2 contains a literature review on the subject of two-phase distribution in compact heat exchanger manifolds. As a basis for understanding the manifold distribution issue, an introduction to flow regime maps in small diameter tubes are presented.

MPE-tube heat exchanger manifolds

Yoo et al. (2002) conducted air-water experiments on a horizontally and vertically oriented manifold with fifteen MPE-tubes (this work was also partially published by Tompkins et al. (2002b)). The MPE-tubes were 6-port aluminum tubes with a flow cross sectional area of $1.669 \times 10^{-5} \text{ m}^2$. The tubes did not protrude into the manifold. Air flow distribution, water distribution and pressure profiles along the manifold were measured. The area ratio, defined as the sum of the branch tube cross-sectional area divided by the cross-sectional area of the manifold, was changed by adjusting the height of the rectangular tube manifold. Four different entrance locations were employed to the manifold. Maldistribution was generally seen to increase at increasing inlet mass flux. At low inlet mass fluxes, the flow pattern in the manifold was stratified-wavy, and the water was preferentially distributed to the first tubes in the manifold.

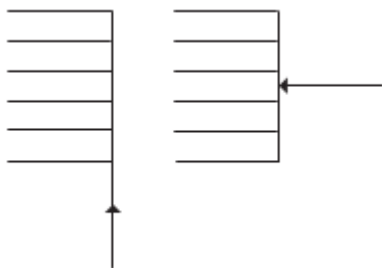
At high mass fluxes, annular flow was observed in the manifold and the liquid film at the bottom entered the first MPE-tube, while the remaining liquid film around the periphery of the manifold reached the end of the manifold and entered the last MPE-tubes. Generally, the air flow distribution was inversely related to the water flow distribution. The authors cited that the liquid film on the walls was moved along the manifold by the vapour drag. No correlation was found between the pressure profile along the manifold and the air/water distribution. Various parameters were utilized in an attempt of reducing the experimental data, but no universal trends were discovered. However, it was seen that the tests with short inlet lengths to the manifold produced more maldistribution than the tests with longer inlet lengths. Vapour fraction and mass flux at the inlet of the manifold did not have big impact on the normalized standard deviation values of the air/water distributions. Tompkins et al. (2002a) developed a mathematical model based on the data given in Yoo et al. (2002). This model is outlined in Section 2.7.2.

Stott et al. (2002) used a MPE-tube evaporator with feeding of the two-phase flow at four locations along the inlet manifold. Measurement of superheat at the outlet of the tubes were used to quantify maldistribution. Capacity reduction due to maldistribution in the evaporator was estimated to 13% at dry conditions and 19% at wet-coil conditions.

Song and Bullard (2002) observed frosting patterns as a qualitative indicator of maldistribution of CO_2 in a multipass MPE-tube evaporator with vertical manifolds and horizontal branch tubes. The tubes at the bottom or at the top of the manifold usually received less liquid than the others. Location of these tubes was determined by a balance between inertial, gravitational and shear forces. In the first passes, containing most liquid, the gravitational forces were dominant, while moving downstream the inertia forces became more important in determining the flow distribution.

It was seen that the refrigerant maldistribution created non-uniform frost deposition, which increased air velocity through the regions where the surface was unfrosted.

Cho et al. (2002) studied two-phase R-22 maldistribution in a vertical manifold with fifteen horizontal MPE-tubes. Two solutions for the inlet to the manifold were tested. First, in the inline configuration (Figure 2.1 a)) the inlet tube had the same direction as the manifold, with vertical upward flow. Second, in parallel configuration (Figure 2.1 b)), the vertical manifold was fed with a horizontal inlet pipe at the middle of the manifold. The inlet pipe was then parallel to the heat exchanger MPE-tubes. The flow maldistribution improved when changing from parallel to inline configuration. For both configurations, the mass flow rate was largest in branch tubes at the bottom of the manifold. The difference in phase separation ratios for the MPE-tubes decreased as the inlet vapour fraction increased.



a) Inline configuration b) Parallel configuration

Figure 2.1: Inline and parallel manifold inlet configuration used by Cho et al. (2002).

Lee and Lee (2002) investigated two-phase distribution in a vertical manifold (24 mm × 24 mm) with six horizontal flat branch tubes (22 mm × 1.8 mm). The branch tube protrusion depth could be varied from 0 to 12 mm into the manifold. Air and water were used as test fluid. Deeper protrusion prevented the water from entering the first branch tubes of the manifold. A protrusion depth of 3 mm was found to give most uniform liquid distribution.

Zietlow et al. (2002) presented an experimental setup with the purpose to measure liquid distribution in a MPE-tube manifold. Further details regarding the measurement concept is given in Section 3.2.1.

2.4 .Two-phase flow patterns in horizontal pipe flow

As pointed out in the previous Section, several authors mentioned that the flow pattern at the inlet of the manifold and along the manifold length was of great importance for the two-phase distribution. Therefore, it is useful to consider the flow patterns which occur in two-phase flow in pipes as a basis for understanding the flow patterns of the developing flow in the manifold. One complication in the analysis of horizontal pipe flow compared to vertical flow is that the flow is not symmetrical around the axial centre axis. The flow patterns that can be observed in horizontal two-phase flow are shown in Figure 2.2.

Bubbly flow:

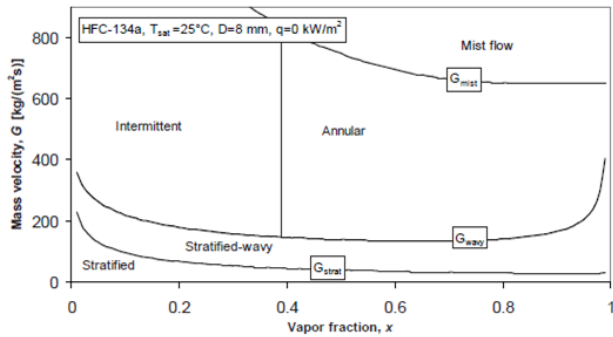
At low gas flow rates, the gas is distributed in discrete bubbles in a continuous liquid phase. The bubbles tend to flow in the upper part of the tube due to buoyancy.

Plug flow (elongated bubble flow):

An increase in gas flow rate cause the bubbles to coalesce into large elongated plug-type bubbles, which flow in a continuous liquid phase in the upper part of the tube.

Slug flow:

The liquid flow is contained in liquid slugs, separating successive gas bubbles. The length of the gas bubbles can vary considerably and contain liquid droplets. Gas bubbles may be dispersed in the liquid slug.



2.5.1. Definitions

When studying the available literature on two-phase split in T-junctions, it is useful to first establish some definitions, Figure 2.4.

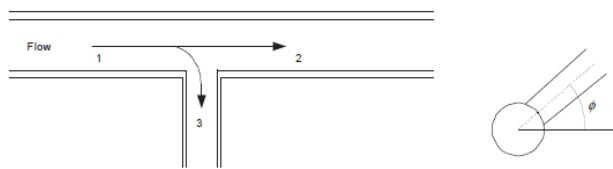


Figure 2.4: T-junction conventions.

The T-junctions considered in the present survey has one inlet pipe and two outlet pipes. One of the outlet pipes is in line with the inlet pipe, and the third pipe, often denoted as the branch or the side arm, meet the main pipe in a right angle.

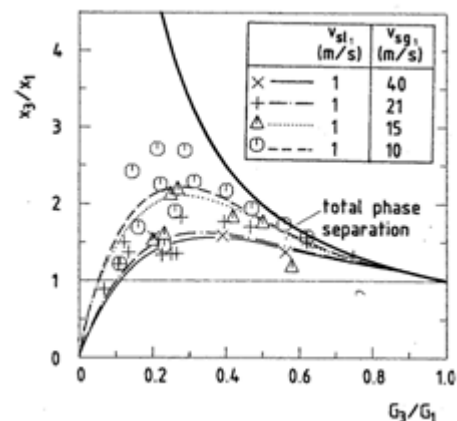
The diameter of the branch, D_3 , is generally not equal to D_1 . The angle denotes the angle between the axial direction of the branch and the horizontal plane, see Figure 2.4.

Most T-junctions used in research have been machined from solid material and therefore have no rounding of the T-junction corners:

Details of sources for experimental data on T-junctions with horizontal main pipe and 90° angle between the main pipe and the branch tube.

Sources	D_1 (m)	D_3/D_1	(deg)	ρ_1 (bar)	u' (m/s)	u'' (m/s)
Orange (1973)	0.076	0.67, 1.0	0°	30	3-14	0.00018
Fouada and Rhodes (1974)	0.051	0.5	+90°	1.5	24-51	0.046-0.077
Collier (1976)	0.038	0.67	0°	3.0	0.8-18.5	0.066-0.13
Hong (1978)	0.0095	1.0	0°	1.2-1.6	9.43	0.0023-0.047
Henry (1981)	0.1	0.2	0°	1.0	25-100	0.1-0.8
Azzopardi and Whalley (1982)	0.032	0.4	0°	2.5	21	0.08
			±30°			
			±60°			
			±90°			
Saba and Lahey (1984)	0.038	1.0	0°	1.3-1.9	0.8-6.5	1.35-2.7
Hwang and Lahey (1988)						
Reimann and Kalm (1984)	0.206	0.03-0.15	-90°	5	0-1.65	0.02-0.3
Seeger et al. (1985)	0.05	1	0°	4-100	4.40	0.5-4
Seeger et al. (1986)			±90°			
Smoglie and Reimann (1986)	0.206	0.03-0.1	0°	5.0		
			±90°			
Shoham and Brill (1987)	0.051	0.5, 1.0	0°	3.0	2.7-26	0.011-0.055
Shoham et al. (1989)						
Katsounis (1987)	0.203	0.26	+90°	1.0	0.03-2	0.025-1.7
Rübel et al. (1988)	0.038	1.0	0°	1-2.5		
Reimann et al. (1988)	0.05	0.08	0°	4-100		
		1.0	±90°			
Ballyk et al. (1988)	0.026	0.5	0°	1.1-2.1		
Peng et al. (1996)		0.82	-45°			
Shoukri et al. (2002)		1.0	-90°			
Azzopardi and Memory (1989)	0.038	0.33	+90°	1.5-3.0	0.7-31	0.008-0.078
Azzopardi and Smith (1992)			0°			
Azzopardi (1999)						
Hart et al. (1991a)	0.05	0.75	0°	1.0	7-10	0.00007-0.031
Hart et al. (1991b)			+0.25°			
Ottens et al. (1999)			+0.5°			
Middle et al. (1993)	0.23	0.43	+90°	1.0	0.01-0.19	0.5-1.5
Buell et al. (1994)	0.038	0.206	0°	1.5-3.0	2.7-40	0.002-0.18
Walkers et al. (1998)		0.5				
Roberts et al. (1995)	0.127	0.6	0°	1.0	4.43	0.0045-0.558
Rea (2001)		1.0	+90°			
Went et al. (1999)						
Pannatcha et al. (1996)	0.5	0.5	-60°	3.0	6.1	0.003-0.059
Matti and Shoham (1997)		1.0	+35°			
Peng et al. (1998)	0.076	0.33-1.0	0°	1.1-1.6	1.5-5	0.05-0.9
			-90°			
Stacey et al. (2000)	0.005	1.0	0°	1.5	48-80	0.1-0.2
Tae and Cho (2003)	0.00812	0.61, 1	0°	6.5	0.74-7.4	0.09-3.38
			±90°			

In Figures 2.6 to 2.9 examples of results from (Seeger et al., 1985) are shown. Phase separation was presented by plotting the ratio of branch tube to main tube inlet vapour fraction, x_3/x_1 , against the total flow split, G_3/G_1 . Equal phase distribution was then represented by the horizontal line $x_3/x_1 = 1.0$.



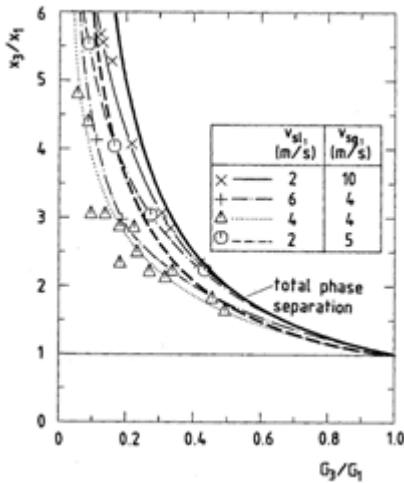


Figure 2.6: Phase separation for horizontal branch tube. Air-water, $D_1 = D_3 = 50$ mm, $P_1 \approx 0.7$ MPa, $u^S = \text{const}$. Reproduced from (Seeger et al., 1985).

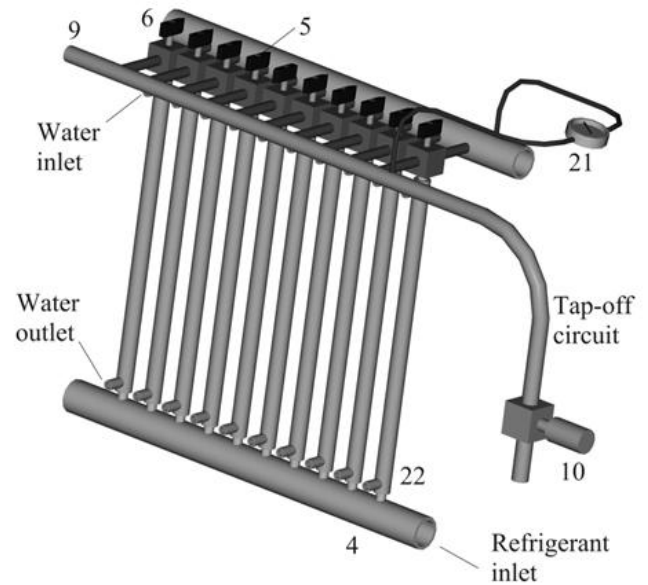


Table 3.1: Test rig instrumentation summary

Location	Type of instrument	Fig 3.1
Electric power,	Watt transducer,	$Q_{ph} \pm 14.1W$
Refrigerant temperature,	Thermocouple type E,	T_{phIn}
Refrigerant temperature,	Thermocouple type E,	T_{cOut}
Water temperature,	Thermocouple type E,	$T_{w,cIn}$
Water temperature,	Thermocouple type E,	$T_{w,cOut}$
Water temperature,	Thermocouple type E,	$T_{w,t sIn}$
Water temperature,	Thermocouple type E,	$T_{w,t}$
Refrigerant pressure,	Gauge pressure transmitter,	P_{mIn}
Refrigerant pressure,	Gauge pressure transmitter,	P_{cIn}
Refrigerant pressure,	Gauge pressure transmitter,	P_{mIn}
Refrigerant pressure,	Gauge pressure transmitter,	P_{cIn}
Manifold differential	Differential pressure	$dpm \pm 0.15\%$
Mass flow refrigerant,	Coriolis type, Rheonik	\dot{m}_{mIn}
Mass flow refrigerant,	Coriolis type, Rheonik	$\dot{m}_{t,i}$
Mass flow water,	Coriolis type, Rheonik	$\dot{m}_{w,c}$
Mass flow, water circuit	Coriolis type, Rheonik	$\dot{m}_{w,t s}$

